

Search for Supersymmetry in opposite-sign same-flavour dilepton events with the CMS detector in proton-proton collisions at

$\sqrt{s} = 8 \text{ TeV}$

Von der Fakultät für Mathematik, Informatik und Naturwissenschaften der RWTH Aachen University
zur Erlangung des akademischen Grades eines Doktors der Naturwissenschaften genehmigte
Dissertation

vorgelegt von
Jan-Frederik Schulte, M.Sc.
aus Münster

Berichter:
Prof. Dr. Lutz Feld
Prof. Dr. Michael Krämer

Termin der mündlichen Prüfung: xx.xx.2015

Diese Dissertation ist auf den Internetseiten der Hochschulbibliothek
online verfügbar.

Zusammenfassung

Abstract

Contents

Zusammenfassung	i
Abstract	i
1 Introduction	1
2 The Standard Model and its extension to Supersymmetry	3
2.1 The Standard Model of particle physics	3
2.2 Motivation for extending the Standard Model and Supersymmetry	3
2.3 Production of lepton pairs in supersymmetric models	3
2.4 Kinematic edges in the dilepton invariant mass spectrum	3
3 Experimental setup	5
3.1 The CERN Large Hadron Collider	5
3.2 The CMS detector	6
3.2.1 The tracking system	6
3.2.2 The electromagnetic calorimeter	9
3.2.3 The hadron calorimeter	10
3.2.4 The muon system	11
3.3 Data acquisition and event reconstruction	13
4 Data analysis and event selection	15
4.1 Trigger and event processing	15
4.2 Object reconstruction	15
4.3 Datasets	15
4.4 Event selection	15
5 Estimation of Standard Model backgrounds	17
5.1 Flavour-symmetric backgrounds	17
5.2 Backgrounds containing a Z boson	17
5.3 Investigation of possible further backgrounds	17
5.4 Search for a kinematic edge with a fit	17
6 Results	19
6.1 Result of the counting experiment	19
6.2 Result of the search for a kinematic edge	19
7 Interpretation in simplified models	21
7.1 Simplified Models for Supersymmetric Signatures	21
7.2 The T6bbledge and T6bbslepton model	21
7.3 Interpretation of the counting experiment in simplified models	21
8 Outlook to LHC Run II	23
9 Conclusion	25

1 Introduction

2 The Standard Model and its extension to Supersymmetry

2.1 The Standard Model of particle physics

2.2 Motivation for extending the Standard Model and Supersymmetry

2.3 Production of lepton pairs in supersymmetric models

2.4 Kinematic edges in the dilepton invariant mass spectrum

3 Experimental setup

3.1 The CERN Large Hadron Collider

The Large Hadron Collider (LHC) [1], located at CERN near Geneva and stretching far into the french countryside, is capable of colliding protons and lead ions at higher energies than any of its predecessors. Also the instantaneous luminosity delivered to the experiments exceeds that of any previous machine at the energy frontier. It was constructed in the tunnel formerly inhabited by the LEP electron-positron collider in 100 m depths below the surface with a circumference 27 km. It was designed to collide protons at a centre-of-mass energy of $\sqrt{s} = 14 \text{ TeV}$ with instantaneous luminosities of $10^{34} \text{ s}^{-1} \text{ m}^{-2}$.

The LHC consists of eight arcs, as shown in Figure 3.1, where superconducting dipole magnets are used to provide a magnetic field of up to 8.3 T at the highest planned energies to bend the charged particles along the curvature of the tunnel, while quadrupole and other specialised magnets are used to focus the beams. In straight segments between these arcs, LHC infrastructure and the experiments are located. The infrastructure components include the cooling facilities necessary to reach a temperature of 1.9 K around the ring, the superconducting cavities in which the protons are accelerated by standing electromagnetic waves, collimators for beam cleaning and the beam dump, where the beam is ejected from the LHC at the end of fills. In the other four straight segments the beam is brought into collisions, which are studied by the four large experiments at the LHC. Of these, CMS [2] and ATLAS [3] are multi-purpose detectors with a diverse physics program, while ALICE [3] and LHCb [4] are more narrowly focused on heavy ion collisions and flavour physics, respectively.

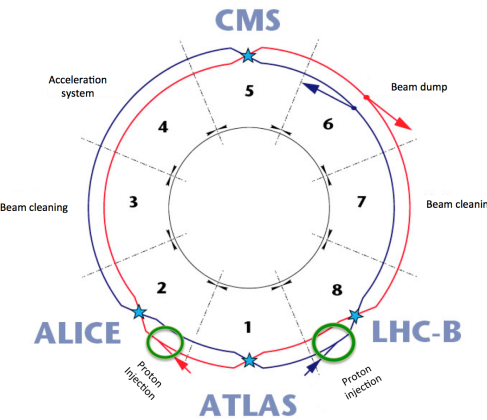


Figure 3.1: Schematic view of the LHC with its eight arcs. The four interaction points, where the experiments are located, are marked with blue stars. Other important parts of the LHC infrastructure are also indicated [5].

The protons circulating the LHC are injected at an energy of 450 GeV after running through a chain of pre-accelerators, the Linac2, the Proton Synchrotron Booster (PSB), the Proton Synchrotron (PS) and the Super Proton Synchrotron (SPS). The proton beams are separated into bunches of about 10^{11} particles. Though being 25 ns by design, corresponding to up to 2808 bunches in the LHC, the smallest spacing between bunches in time was 50 ns throughout the running in 2012 and most of 2011. In

these running conditions, after three years of running in the years 2010 to 2012, constituting the so called Run I of the LHC, a centre-of-mass energy of $\sqrt{s} = 8 \text{ TeV}$ has been reached. The instantaneous luminosities delivered to the experiments reached a maximum of $7.7 \cdot 10^{33} \text{ s}^{-1} \text{ m}^{-2}$ in late 2012, as can be seen on the left side of Figure 3.2. The integrated luminosity delivered to the CMS experiments in 2012 was 23.3 fb^{-1} , exceeding that of 2011 by almost a factor of four [6], as shown on the right side of Figure 3.2.

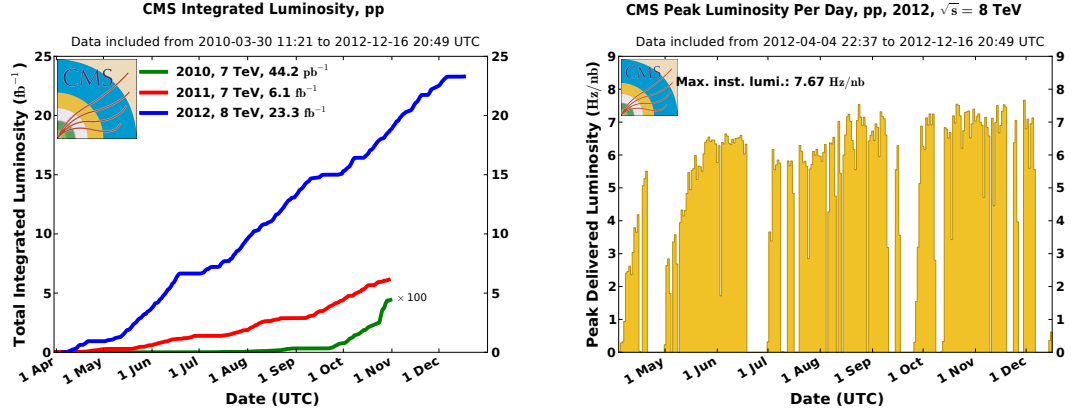


Figure 3.2: Development of instantaneous (left) and integrated (right) luminosity delivered to the CMS experiment. The left plots shows the results for all three years of data taking, while the right one only shows the 2012 data taking.

3.2 The CMS detector

Located in one of the four intersections of the LHC beams, the CMS detector is designed to measure the resulting collisions to high precision. Key ingredients are a high precision measurements of the properties of single particles as well as a good coverage of the 4π solid angle. The central element of the CMS detector is a superconducting solenoid. Cooled to 4.45 K , it is able to produce a homogeneous magnetic field of 3.8 T , which allows to measure the momentum of charged particle by bending their trajectories. As shown in Figure 3.3, the different components of the detector are layered in cylindrical shapes around the interaction point. The magnet encompasses most of the main subdetectors, namely the tracking system which measures the trajectories of charged particles and the electromagnetic and hadron calorimeters, designed to measure the energy of particles. Located outside of the volume of the solenoid are the iron return yoke and muon detectors. This cylindrical structure is complemented on both sides by endcaps, which close the solid angle in the direction of the beams and are partly located outside the volume of the solenoid. The different components are described in more detail in the following.

3.2.1 The tracking system

The trajectory of charged particles can be determined by measuring the signal of the ionization they cause when traversing matter. The tracking system of the CMS detector consists of many layers of silicon pixels and strips. Combining the points at which a charged particle traverses the different layers, the trajectory of this particle can be measured. The bending of this trajectory under the influence of the magnetic field allows to determine the momentum of the particle. The tracking system has a diameter of 2.5 m and a length of 5.8 m , corresponding to a geometric coverage of $|\eta| < 2.5$. The

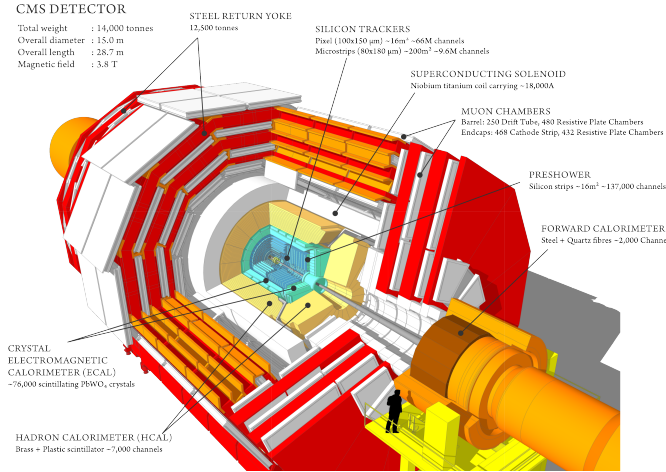


Figure 3.3: Schematic view of the CMS detector [7]. From the inside out, the tracking system is shown in blue, the electromagnetic calorimeter in green, the hadron calorimeter in light yellow, the superconducting solenoid in white, the return yoke in red and the muon system again in white.

tracking detector consists, as shown in Figure 3.4, of the pixel detector (PIXEL) surrounded by various components of the silicon strip tracker.

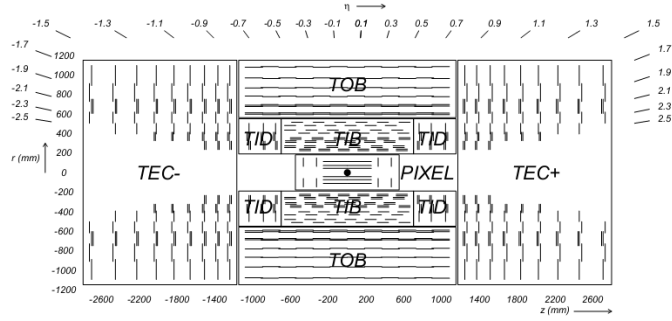


Figure 3.4: Schematic view of the CMS tracking detector. The innermost part shows the pixel detector (PIXEL), surrounded by the tracker inner barrel (TIB) and tracker inner discs (TID). The outermost parts of the tracking detector are the tracker outer barrel (TOB) and the two tracker endcaps (TEC+ and TEC-).

The silicon pixel detector

The innermost part of the tracking system is the pixel detector, which consists of three layers in the barrel region at radii between 4.4 cm and 10.2 cm, complemented by two discs perpendicular to the beam axis, located at $|z| = 34.5$ cm and $|z| = 46.5$ cm. As the particle density is highest close to the interaction point, a high granularity is needed to maintain a low occupancy of the pixel detector. Therefore the pixel detector consists of roughly 66 million pixels with a combined active area of about 1 m 2 . Each pixel has a size of 150 \times 100 μm^2 . The analogue readout of the pixels allows to combine the measurements of neighbouring pixels, bringing the spatial resolution down to 15 to 20 μm . This is especially important for the reconstruction of the interaction vertices and the tagging of the secondary vertices from the decay of b-hadrons.

The silicon strip detector

Further away from the interaction point, between 20 cm and 116 cm, the granularity of the tracking system is reduced. Silicon strip detectors are used, structured in four layers of the tracker inner barrel (TIB), complemented on each side with three discs of the tracker inner discs (TID). All this is surrounded by the six layers of the tracker outer barrel (TOB). The tracker endcaps (TECs) consist of nine discs each. The individual strips have a length of about 10 cm and a pitch between 80 μm in the two inner layers of the TIB and 183 μm in the four inner layers of the TOB. The single point resolution in TIB and TOB depends on the layout of the specific layer and varies between 23 μm and 53 μm .

Stereo modules, constructed by placing two modules back to back, rotated by 100 mrad, are placed in the first two layers of both TIB and TOB, the first two discs of TID and the first two and the fifth discs of the TECs. These allow for 2-D measurements, with a precision of the z position measurement of 230 μm in TIB and 530 μm in TOB.

For high momentum tracks of about 100 GeV in the region of $|\eta| < 1.6$ a p_T resolution of 1-2% is achieved, while the impact parameter of these tracks can be measured with a resolution of about 10 μm .

Compared to other tracking technologies, an all silicon tracking system as used in CMS consists of significantly more material. The material budget lies between 0.4 and 1.8 radiation length X_0 , as shown in Figure 3.5. For light charged particles such as electrons this leads to a significant probability to emit bremsstrahlung in while traversing the tracking detector, which has to be taken into account in the reconstruction of particles.

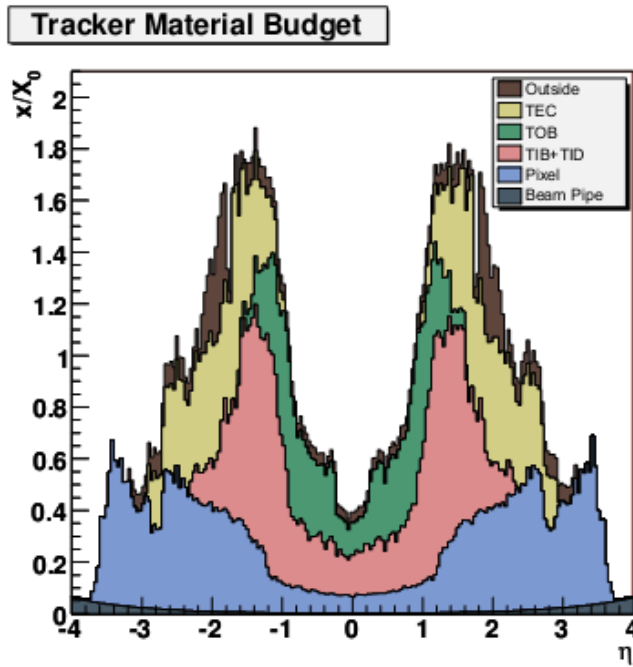


Figure 3.5: Material budget of the CMS tracking detector in units of radiation length X_0 as a function of η .

3.2.2 The electromagnetic calorimeter

The electromagnetic calorimeter (ECAL) measures the energy of electrons and photons. It uses lead tungstate ($PbWO_4$) crystals both as absorber and active material. The electromagnetic shower induced by the electron or photon leads to the emission of scintillation light in the crystal, which is measured at the end of the crystals by avalanche photo diodes (APDs) in the barrel segment of the ECAL and more radiation hard vacuum photo triods (VTPs) in the endcap region. The choice of lead tungstate was driven by the need for a material that is at the same time dense (8.28 g/cm^3), has a small Molière radius (2.2 cm) and is fast. About 80% of the scintillation light is emitted after 25 ns, which is the time between two LHC bunch crossing under design conditions. The structure of the ECAL is shown

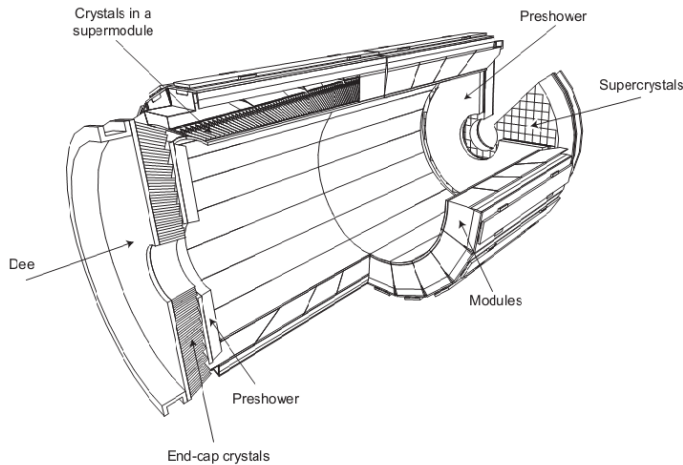


Figure 3.6: Schematic view of the CMS ECAL.

in Figure 3.6. The ECAL barrel (EB) covers the region of $|\eta| < 1.479$ and consists of 61200 crystals. They have a size of $2.2 \times 2.2 \text{ cm}^2$ at the front and $2.6 \times 2.6 \text{ cm}^2$ at the back, with a length of 23 cm, corresponding to $25.8 X_0$. In the ECAL endcaps (EE), consisting of 7324 crystal each, they are slightly larger ($2.862 \times 2.862 \text{ cm}^2$ to $3.0 \times 3.0 \text{ cm}^2$) and shorter (22 cm, corresponding to $24.7 X_0$). The EE extend the geometric coverage of the ECAL to $|\eta| = 3.0$.

In the region of $1.653 < |\eta| < 2.6$ a preshower detector, consisting of two layers of silicon strips and two layers of lead absorber, is installed to distinguish between prompt photons and those from the decay $\pi^0 \rightarrow \gamma\gamma$. The strips, oriented perpendicular to each other, have a pitch of 2 mm, allowing to resolve the two showers of the photons from the π^0 .

The production of scintillation photons per energy deposit is temperature depend. Therefore the ECAL is kept at a temperature of $18 \pm 0.05^\circ\text{C}$, where it is about 4.5 photons per MeV.

The typical resolution of the ECAL is parametrized as

$$\left(\frac{\sigma}{E}\right)^2 = \left(\frac{2.8\%}{\sqrt{E}}\right)^2 + \left(\frac{0.12}{E}\right)^2 + (0.30\%)^2, \quad (3.1)$$

with three terms describing different sources of uncertainty. The first term includes statistical fluctuation in the production of scintillation light as well as the energy distribution over several crystals. The second term covers such sources of noise as electronic noise or pileup. The constant term accounts for other sources of uncertainties such as calibration errors. The size of the different contributions has been confirmed in test beam measurements [8].

3.2.3 The hadron calorimeter

The hadron calorimeter (HCAL) measures the energy of charged and neutral hadrons. In the barrel region of the detector it is situated between the back face of the ECAL and the coil of the solenoid, at radii between 1.7 m and 2.95 m, limiting the amount of material that can be used in its construction. Therefore additional detectors are placed outside of the volume of the magnet, forming the hadron outer calorimeter (HO). The HCAL barrel (HB) is complemented on each side by a HCAL endcap (HE) and the geometric coverage is extended to high values of $|\eta|$ by dedicated forward calorimeters (HF). The placement of these subdetectors relative to the other components of CMS are shown in Figure 3.7.

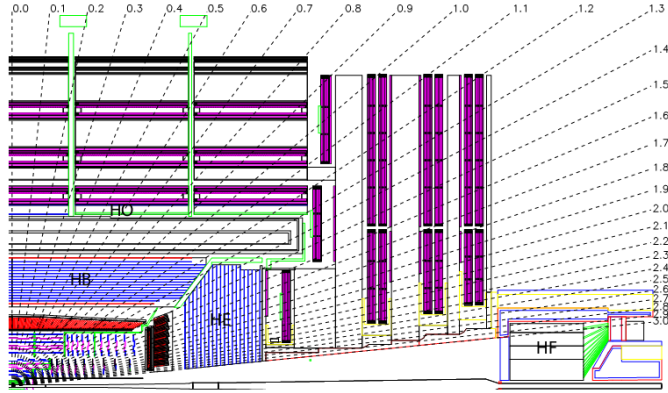


Figure 3.7: Schematic view of the CMS HCAL.

The HCAL barrel and outer detectors (HB and HO)

The HB covers the geometric region $|\eta| \leq 1.3$. It is constructed as a sandwich calorimeter, consisting of plastic scintillator as the active material. For the absorber material, the fourteen inner layers of the HB are made from brass, while steel is used for the front and back plates of the HB to increase the stability of the construction. The scintillator is divided in 144 segments in ϕ and 32 segments in η , resulting in a spatial granularity of 0.087 in both η and ϕ . The scintillation light produced in the active material is transported to hybrid photo diodes using scintillating fibres. As all layers of one tower in η and ϕ are read out by the same photo diode, there is no segmentation in the readout in r , except for the two towers closest to the HE on each side. The material of the ECAL in front of the HB corresponds to about 1.1 interaction length λ_i . The absorber material of the HB itself amounts to only 5.82 λ_i at $\eta = 0$, which increases to 10.6 λ_i at $|\eta| = 1.3$. To measure the energy of jets not contained in the HB, the HO is placed outside the vacuum containment of the solenoid. It consists of one additional layer of scintillator, with the magnet acting as absorber, except for most central part of the detector, where one additional layer of steel absorber and scintillator are installed. Hereby the material budget of the HCAL is increased to at least 10 λ_i over the whole barrel region.

The HCAL endcaps (HE)

The HE extends the geometric coverage of the HCAL up to $|\eta| = 3.0$, coinciding with that of the EEs. It is constructed from the combination of brass absorber and plastic scintillator as the HB and for the region $1.3 \leq |\eta| \leq 1.6$ also retains the $\Delta\eta \times \Delta\phi = 0.087 \times 0.087$ granularity in η and ϕ . For $|\eta| \geq 1.6$ the segmentation is coarser, resulting in a granularity of $\Delta\eta \times \Delta\phi \approx 0.17 \times 0.17$. This structure again corresponds to about $10 \lambda_i$. The longitudinal segmentation of the readout of the towers differs based on the location of the tower. The two towers closest to the beam line are read out in three segments, while most others are read out in two segments. The two towers overlapping with HB are read out without longitudinal segmentation. Multipixel hybrid photo diodes have been chosen for the readout due to their low sensitivity to magnetic fields.

The hadron forward calorimeter (HF)

Of all subdetectors of CMS, the HF covers the highest values of $|\eta|$, reaching up to values of $|\eta| = 5.2$. This close to the beam pipe radiation hardness is the key feature of the design, as nearly 90% of the energy deposited in the detector as the result of a proton-proton interaction is allotted to the HF. It is constructed as two 3.5 m long cylinders with a radius of 1.3 m, located at $|z| = 11.2$ m. The first 1.65 m consist of plates of steel with a thickness of 5 mm, again corresponding to about $10 \lambda_i$. The active material are quartz fibres, which are inserted into grooves in the steel plates. The particles created in showers in the absorber emit Cherenkov radiation in the fibres, which is detected by photomultiplier tubes at the end of the fibres. As the Cherenkov threshold is lowest for electrons, at 190 keV, the HF is more sensitive towards electromagnetic than hadronic showers. To separate the two, half of the fibres start only at a depth of 22 cm inside the absorber. As the electromagnetic shower develops faster, they deposit most of their energy before this point, which distinguishes them from hadronic showers.

3.2.4 The muon system

Muons are in general not stopped by any of the subdetectors of the CMS detector inside the solenoid. Therefore they can be measured with high precision in a clean environment outside of it. The muon detectors are therefore placed inside the return yoke of the magnet, both for the muon barrel (MB), covering up to $|\eta| = 1.2$ and muon endcap (ME) detectors, placed between $|\eta| = 0.9$ and $|\eta| = 2.4$. Being placed so far away from the interaction point, the muon detector have to cover a large area, which requires them to be rather inexpensive compared to other technologies used in the construction of CMS. Three different types of gaseous detectors are used to provide at the same time identification, p_T measurement and triggering for muons. In the barrel region, drift tubes (DT) are used as the main muon detectors, while in the endcaps cathode strip chambers (CSC) are used because they are faster and better equipped to deal with the larger and inhomogeneous magnetic field in this region of the detector. To provide a very fast muon tagging for the trigger, resistive plate chamber (RPC) complement the other two technologies in both the barrel and the endcaps.

Drift tubes (DT)

In the barrel, the TD chambers, each made of 2 or 3 super layers, which in turns are made up of four layers of TDs, are grouped together into four muon stations. Of these the first three contain 2 groups of 4 layers of chambers measuring in the $r - \phi$ plane and one group measuring the z coordinate. In the last muon station only the groups measuring in $r - \phi$ are present. The chambers in each chamber

are offset by half of the width of a cell with respect to the next layer to not leave dead spots in the geometric coverage. The DT system consists of about 172000 sensitive wires. The drift tubes are filled with a mixture of 85% Ar and 15% CO_2 , and their structure is shown in Figure 3.8. The $r\phi$ resolution of a single layer of DT is about 250 μm , so that one chamber reaches a precision of 100 μm .

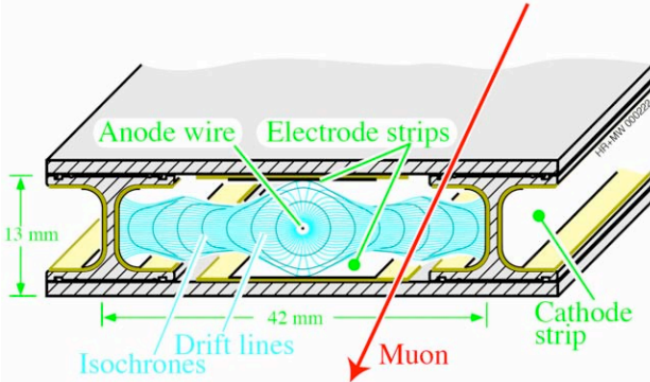


Figure 3.8: Schematic view of one DT.

Cathode strip chambers (CSC)

The CSC are multiwire proportional chambers, consisting of 6 planes of anode wires interleaved with 7 panels of cathode strips. The chambers have trapezoidal shape and are arranged in four discs around the beam axis, each further segmented into two or three rings. The cathode strips measure the ϕ coordinate while the anode wires measure the radial coordinate. Figure 3.9 shows the structure of one chamber on the left side and the creation of a signal due to a amplification of the initial ionization in an avalanche close to the anode wire.

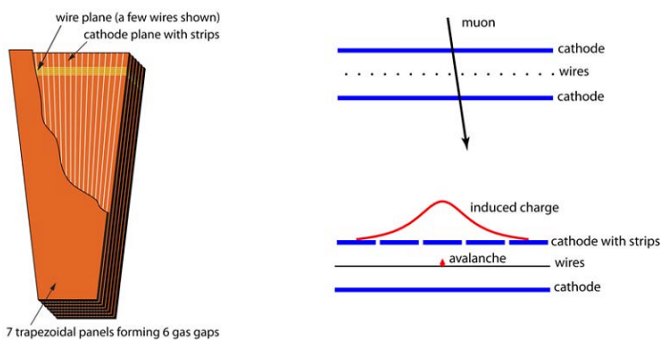


Figure 3.9: Schematic view of one CSC (left) and the creation of a signal (right).

Resistive plate chambers (RPC)

The RPCs consist of three layers of Bakelite, which form two small gas filled gaps and between which high voltage is applied. The amplification of the initial signal is very fast in this configuration, with drift times of about 5 ns. Therefore this technology is well suited to associate muon candidates to the

LHC bunch crossings. In the barrel region six layers of RPCs are installed, while three layers are used in the endcaps for $|\eta| \leq 1.6$.

Momentum resolution

The p_T resolution of the muon system alone was expected to be about 10% for muons with p_T up to 200 GeV. Combined with the information from the inner tracking system, a resolution of about 1% was expected to be achieved in the central region of $|\eta| \leq 0.8$ for a p_T of 10 GeV, increasing to about 2% for a p_T of 200 GeV.

The p_T resolution for muons has been measured using data collected in 2010 [9]. Using the muon system alone, resolutions better than 10% have been found for the barrel region for muons with $p_T > 15$ GeV. The muon resolution improves when combining the information from the muon system with those from the inner tracking system. The precision of the tracking system dominates for a wide p_T range and averaging over η and ϕ resolutions of $(1.8 \pm 0.3(\text{stat.}))\%$ at $p_T = 30$ GeV to $(2.3 \pm 0.3(\text{stat.}))\%$ at $p_T = 50$ GeV have been achieved.

3.3 Data acquisition and event reconstruction

4 Data analysis and event selection

4.1 Trigger and event processing

4.2 Object reconstruction

4.3 Datasets

4.4 Event selection

5 Estimation of Standard Model backgrounds

5.1 Flavour-symmetric backgrounds

5.2 Backgrounds containing a Z boson

5.3 Investigation of possible further backgrounds

5.4 Search for a kinematic edge with a fit

6 Results

6.1 Result of the counting experiment

6.2 Result of the search for a kinematic edge

7 Interpretation in simplified models

7.1 Simplified Models for Supersymmetric Signatures

7.2 The T6bbledge and T6bbslepton model

7.3 Interpretation of the counting experiment in simplified models

8 Outlook to LHC Run II

9 Conclusion

Bibliography

- [1] Lyndon Evans and Philip Bryant. LHC Machine. *Journal of Instrumentation*, 3(08):S08001, 2008.
- [2] CMS Collaboration. The CMS experiment at the CERN LHC. *Journal of Instrumentation*, 3(08):S08004, 2008.
- [3] ATLAS Collaboration. The ATLAS Experiment at the CERN Large Hadron Collider. *Journal of Instrumentation*, 3(08):S08003, 2008.
- [4] LHCb Collaboration. The LHCb Detector at the LHC. *Journal of Instrumentation*, 3(08):S08005, 2008.
- [5] Particle kickers. <https://cds.cern.ch/record/1706606/>. Accessed: 2014-08-06.
- [6] CMS Collaboration. Public CMS Luminosity Information. <https://twiki.cern.ch/twiki/bin/view/CMSPublic/LumiPublicResults?rev=101>. Accessed: 2014-08-06.
- [7] Cms detector design. <http://cms.web.cern.ch/news/cms-detector-design>. Accessed: 2014-08-08.
- [8] CMS Collaboration. Electromagnetic calorimeter calibration with 7 TeV data. 2010. CMS Physics Analysis Summary EGM-10-003.
- [9] CMS Collaboration. Performance of CMS muon reconstruction in pp collision events at $\sqrt{s} = 7$ TeV. *J. Instrum.*, 7(arXiv:1206.4071. CMS-MUO-10-004. CERN-PH-EP-2012-173):P10002. 81 p, Jun 2012. Comments: Submitted to the Journal of Instrumentation.